Research in Pharmaceutical Sciences, June 2026; 21(3): 278-291
Received: 17-11-2025
Peer Reviewed: 02-12-2025
Revised: 19-01-2026
Accepted: 27-01-2026
Published: 10-05-2026

School of Pharmacy & Pharmaceutical Sciences
Isfahan University of Medical Sciences

Original Article

New 5-(pyridin-3-yl)-1,3,4-oxadiazoles derivatives as VEGFR2 inhibitors: *in silico* study, synthesis, and cytotoxicity evaluation

Ahmed Nasser Abdulhussein* **and Mohammed Abdulameer Oleiwi**

Department of Pharmaceutical Chemistry, College of Pharmacy, University of Baghdad, Baghdad, Iraq

Abstract

Background and purpose: Angiogenesis, regulated by vascular endothelial growth factor receptor 2 (VEGFR-2), has a key role in tumor progression, especially in common cancers, including colorectal and renal cancer. Inhibiting VEGFR-2 is a promising therapeutic approach. This research aimed to design, synthesize, and biologically evaluate new 5-(pyridine-3-yl)-1,3,4-oxadiazole derivatives as potential VEGFR-2 inhibitors.

Experimental approach: A new series of derivatives (AM3-AM6) was synthesized through S-alkylation of 5-(pyridin-3-yl)-1,3,4-oxadiazole-2-thiol and hydrazinolysis reactions, followed by condensation with aldehydes. The compounds were analyzed using FT-IR, ^{1}H-NMR, and ^{13}C-NMR spectroscopy. Molecular modelling studies, including docking (PDB ID: 4ASD), ADMET prediction, and molecular dynamics (MD) simulations, were performed to evaluate binding affinity, pharmacokinetic properties, and complex stability. Cytotoxicity was assessed *via* MTT assay against HT-29 (colorectal), ACHN (renal), and L929 (normal) cell lines.

Findings/Results: Docking results revealed strong binding to VEGFR-2, with compound AM3 showing the best docking score (ΔG = -11.613 kcal/mol). MD simulations confirmed the high stability of the AM3-VEGFR-2 complex with consistent RMSD values and persistent interactions with GLU885 and ASP1046. *In vitro*, AM4 exhibited a significant cytotoxic effect against HT-29 cells (IC_{50} = 38.94 µM), compared to sorafenib (IC_{50} = 9.73), while all compounds were non-toxic toward L929 cells.

Conclusions and implications: *In silico* and *in vitro* results demonstrated that the new 5-(pyridine-3-yl)-1,3,4-oxadiazole derivatives possess favorable drug-like properties and selective anti-proliferative activity against colorectal and renal cancer cells. These findings suggest that this scaffold is a valuable starting point for developing novel selective VEGFR-2 inhibitors as anticancer agents.

Keywords: Cytotoxicity; 1,3,4-Oxadiazole; Molecular modelling; VEGFR-2.

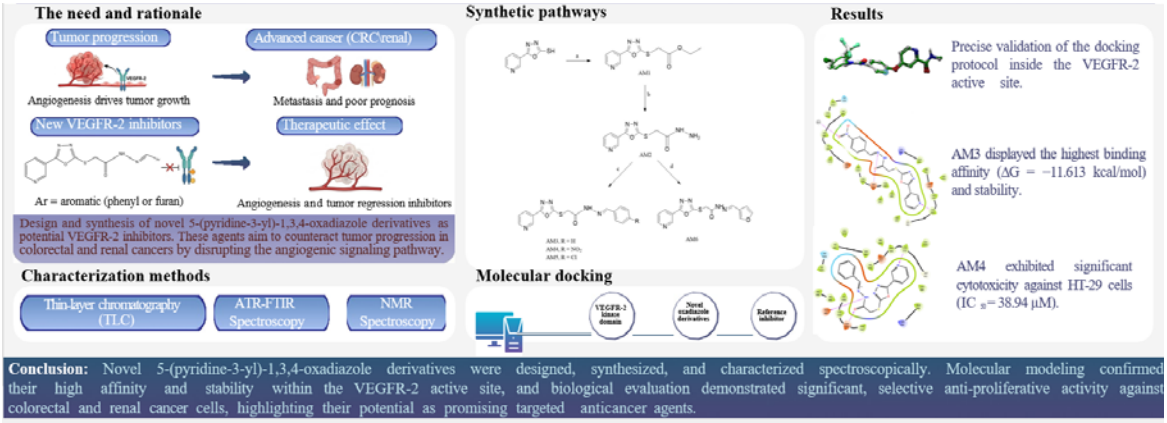

*Corresponding author: A.N. Abdulhussein
Tel: +964-7700825097
Email: ahmed.abd2200@copharm.uobaghdad.edu.iq

Access this article online
Website: http://rps.mui.ac.ir
DOI: 10.4103/RPS.RPS_222_25

INTRODUCTION

Cancer remains a leading cause of mortality worldwide, presenting a formidable challenge to global public health systems. Among the various malignancies, colorectal and renal cancers are particularly concerning due to their rising incidence and high mortality rates (1,2). Despite significant advancements in therapeutic strategies, the prognosis for patients with metastatic disease remains poor, underscoring the critical need for novel, effective, and selective anticancer agents (3).

Central to tumor growth and metastatic dissemination is the process of angiogenesis, the physiological formation of new blood vessels from pre-existing vasculature. This process ensures the supply of oxygen and nutrients necessary for tumor proliferation (4).

Consequently, targeting angiogenic pathways has emerged as a pivotal strategy in cancer therapy. The vascular endothelial growth factor (VEGF) signaling pathway, particularly through its interaction with the VEGF receptor-2 (VEGFR-2), is the primary regulator of tumor-induced angiogenesis. Upon activation, VEGFR-2 initiates a cascade of intracellular signaling events that promote endothelial cell proliferation, migration, and survival (5). Therefore, the inhibition of VEGFR-2 kinase activity represents a validated and effective approach to suppress tumor growth by limiting the tumor of its vascular supply (6).

Small-molecule VEGFR-2 inhibitors mainly bind to the receptor's ATP-binding region, where they compete with ATP molecules for binding. Different receptors that employ ATP as their substrate share similarity with VEGFR-2's catalytic domain. As a result, these inhibitors often work on more than one target, affecting not only VEGFR-2 but also other receptors found in other tissues, even healthy ones. The therapeutic advantage results from the overexpression of VEGFR-2 in many cancer cell types (7).

New potential drug candidates are typically designed by utilizing chemical moieties found in known inhibitors to achieve more effective interactions with the target, enhanced selectivity to minimize their side effects, and improve their pharmacokinetic properties, also addressing mechanisms that contribute to drug resistance (8). In the landscape of drug discovery, heterocyclic compounds play a dominant role, with the 1,3,4-oxadiazole scaffold attracting considerable attention. This five-membered heterocyclic ring serves as a versatile pharmacophore and a bioisostere for carboxylic acids, esters, and amides, contributing to improved metabolic stability and pharmacokinetic properties (9).

Derivatives containing the 1,3,4-oxadiazole core have been reported to exhibit a broad spectrum of biological activities, including antimicrobial, anti-inflammatory, and, notably, anticancer effects (9,10). Compounds including this moiety have attained multiple phases of clinical trial or have been approved by the FDA (Fig. 1) (11). Zibotentan was developed for the treatment of lung, ovarian, breast, colon, and, specifically, prostate cancer (12). Raltegravir, an integrase inhibitor for HIV, is utilized alongside other antiretroviral medications for the treatment of AIDS (13). Tiodazosin is utilized in the treatment of hypertension (14). DNL343 is a eukaryotic translation initiation factor 2B (eIF2B) agonist designed for the treatment of neurodegenerative disorders through the modulation of stress granule production. It is presently undergoing phase II/III clinical studies (15). In addition to these important biological characteristics, 1,3,4-oxadiazoles and their derivatives are known for their cytotoxic properties *via* kinases, enzymes, factors, and other molecules (14). Recent studies have highlighted the potential of oxadiazole-based hybrids to act as potent VEGFR-2 inhibitors, interfering with kinase activity through specific binding interactions within the active site (16-18). Building upon these findings and the proven biological significance of nitrogen-containing heterocycles, this study focuses on the design and synthesis of a novel series of 5-(pyridin-3-yl)-1,3,4-oxadiazole derivatives (Fig. 2). By integrating the pyridine moiety, known for its ability to participate in hydrogen bonding, with the oxadiazole scaffold, we aim to enhance the binding affinity towards the VEGFR-2 kinase domain. Herein, we report the synthesis, structural characterization, and *in vitro* cytotoxicity evaluation of these new derivatives against colorectal (HT-29) and renal (ACHN) cancer cell lines. Furthermore, *in silico* molecular docking and molecular dynamics (MD) simulations were employed to provide mechanistic insights into their binding modes and stability within the VEGFR-2 active site.

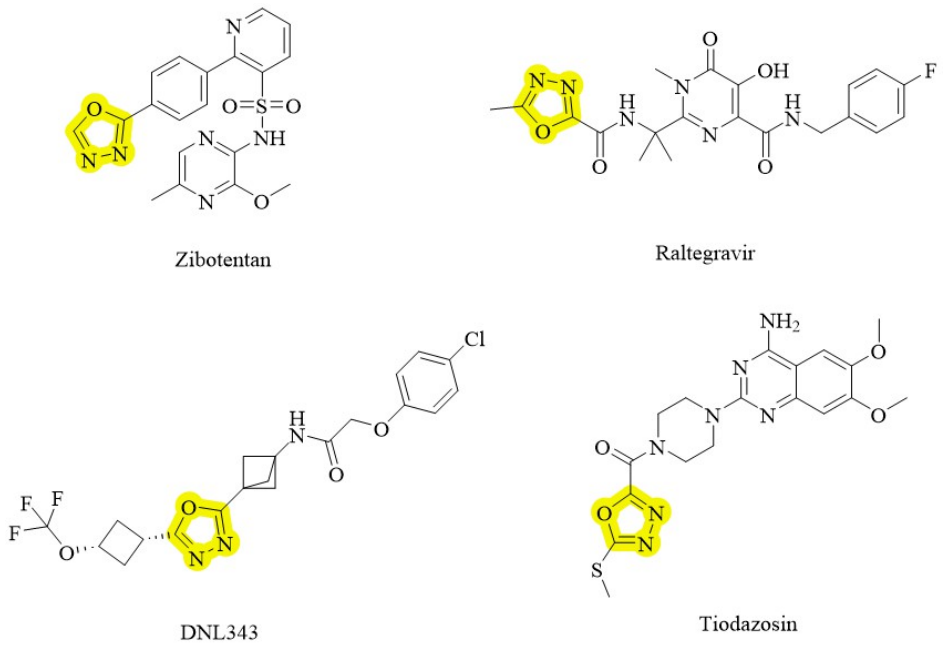

Fig. 1. Examples of compounds with a 1,3,4-oxadiazole ring in their structures.

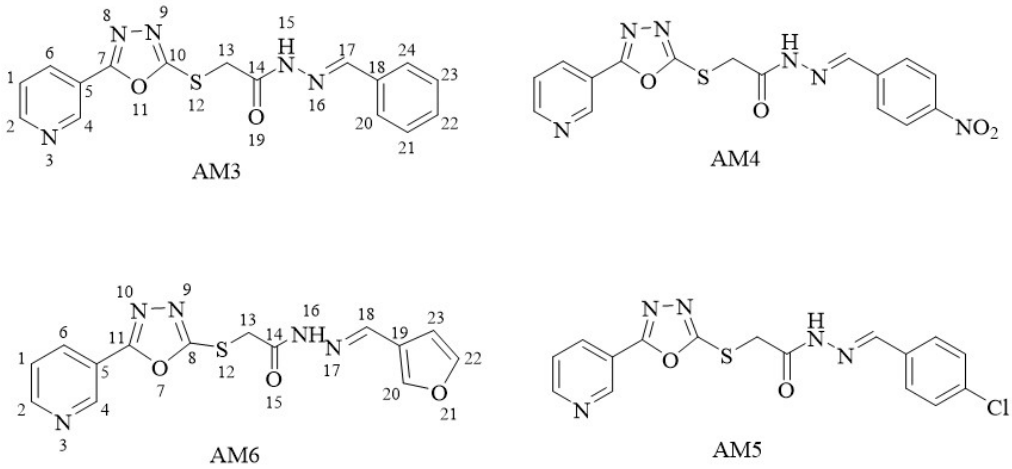

Fig. 2. Chemical structures of the synthesized compounds AM3-AM6. Atom numbering is explicitly shown for the representative compounds AM3 and AM6; the numbering scheme for analogues AM4 and AM5 corresponds to that of AM3.

MATERIALS AND METHODS

Chemistry

All chemicals and solvents were utilized without further purification. All chemicals and solvents were acquired from Merck and Sigma-Aldrich and utilized without additional purification. The parent nucleus (5-(pyridin-3-yl)-1,3,4-oxadiazole-2-thiol) was acquired from Macklin (China). The Stuart CB 162, a German device for determining melting points, was used without any corrections. The infrared spectra of the novel synthesized compounds were obtained utilizing a Shimadzu attenuated total reflectance-fourier transform infrared spectrophotometer (ATR-FT-IR; ύ, cm^{-1}). Proton and carbon nuclear magnetic resonance (^{1}H-NMR and ^{13}C-NMR) spectra were obtained utilizing a Bruker 500 MHz and 126 MHz spectrometer (Bruker, Germany), respectively.

Analytical thin-layer chromatography (TLC) was conducted using Merck silica gel 60 F254 plates with several solvent systems, including hexane: ethyl acetate: methanol in a ratio of 60%: 30%: 10%, and chloroform: ethyl acetate: glacial acetic acid in a ratio of 60%: 30%: 10%.

Synthesis of ethyl 2-((5-(pyridine-3-yl)-1,3,4-oxadiazol-2-yl)thio)acetate (AM1) (21)

The mixture of 5-(pyridin-3-yl)-1,3,4-oxadiazole-2-thiol (5 g, 27.9 mmol) and triethylamine (2.82 g, 27.9 mmol) in 100 mL of water was stirred for 15 min, and then ethyl 2-bromoacetate (4.65 g, 27.9 mmol) was added dropwise over 30 min to the mixture. The mixture was stirred at room temperature for 3 h. The mixture was filtered using a Buchner funnel, followed by multiple washes with water, drying, and recrystallization from 70% ethanol.

Synthesis of 2-((5-(pyridin-3-yl)-1,3,4-oxadiazol-2-yl)thio)acetohydrazide (AM2) (22)

An excess of hydrazine hydrate solution 99.9% (2.83 g, 56.54 mmol) and compound AM1 (3 g, 11.3 mmol) in 50 mL of absolute ethanol was refluxed for 12 h at 78 °C. Upon completion of the reflux period (assessed *via* TLC), the mixture was left to cool down to room temperature, following which the solid product was filtered, rinsed with multiple portions of ethanol, and subsequently dried. Recrystallisation from absolute ethanol yielded the corresponding hydrazide.

General method for the synthesis of compounds AM3-AM6 (22)

A solution of compound AM2 (0.1 g, 0.397 mmol) in 25 mL of absolute methanol, with a few drops of glacial acetic acid as a catalyst, was prepared to which the following aldehydes were added individually. A: Benzaldehyde (0.04 g, 0.397 mmol), B: 4-nitrobenzaldehyde (0.06 g, 0.397 mmol), C: 4-chlorobenzaldehyde (0.05 g, 0.397 mmol), and D: furan-3-carbaldehyde (0.04 g, 0.397 mmol) as illustrated in Scheme 1. The mixture was refluxed for 3-4 h, cooled, and the precipitate was filtered, rinsed with cold methanol, and dried. We used 80% ethanol for recrystallisation to isolate the final chemicals (AM3-AM6).

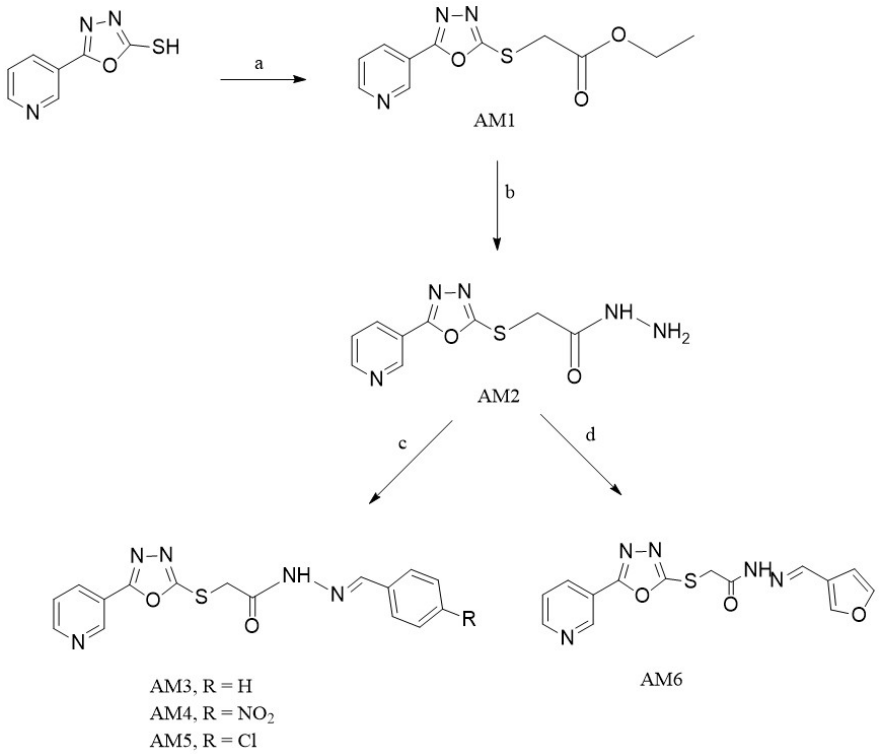

Scheme 1. The general route for the synthesis of the desired compounds (AM3-AM6). a: Ethyl 2-bromoacetate, triethylamine, stirring 3 h at room temperature; b: hydrazine hydrate 99.9%, reflux 12 h; c: 4-substituted benzaldehyde, glacial acetic acid, reflux at 78 °C for 3-4 h; d: furan 3-carbaldehyde, glacial acetic acid, reflux at 78 °C for 3-4 h.

Molecular modelling

The study began with designing twenty-five oxadiazole molecules based on recent research. These molecules were filtered using licensed tools from Maestro Schrödinger's docking and pharmacokinetic property prediction methods.

Molecular docking

The designed molecules were prepared using LigPrep for energy minimization, tautomer generation, and generation of possible ionized forms at pH 7. The Protein Data Bank (PDB) included the crystal structure of the VEGFR2 protein (PDB ID: 4ASD) that was downloaded and prepared *via* the protein preparation wizard. The preparation process included repairing hydrogen, filling in missing chains, removing water molecules larger than 3 Å, and minimizing energy use. To identify each protein's active site using grid generation, the co-crystallized ligands in the protein were exploited.

Standard precision docking was performed utilizing grid-based ligand docking with Glide energy for all compounds targeting the three specified proteins. To further refine the analysis, the compounds exhibiting the highest activity and the best docking scores from standard precision docking were selected for extra precision docking (19).

Pharmacokinetic properties prediction

The most potent compounds were analyzed for their absorption, distribution, metabolism, and excretion (ADME) properties using QikProp within the Schrödinger Maestro software.

MD simulation

MD simulations were conducted on the compound with the highest docking score to assess the stability and compatibility of ligand intercalation within the binding site of VEGFR2 (PDB ID: 4ASD). These simulations utilized Desmond software, integrated into the Maestro interface (Schrödinger Release, 2024). The simulation environment was configured through the System Builder tool, incorporating the simple point charge water model and an orthorhombic periodic box with a 10 Å buffer around the protein's outermost edges. System parameterization leveraged the optimized potentials for liquid simulations (OPLS_4) force field, while sodium and chloride ions were introduced to neutralize the system's charge and maintain a pH-neutral environment. Simulations were executed under isothermal-isobaric "number, pressure, temperature" (NPT) ensemble conditions, maintaining a temperature of 300 K and pressure of 1 bar. The total simulation time spanned 100 ns, with trajectory snapshots recorded at intervals of 50 picoseconds (20).

MTT in vitro cytotoxicity assay

The cell types of L929, ACHN, and HT-29 were introduced to 96-well plates at a density of 5,000 cells per well in 10% fetal bovine serum (FBS) complete media. The cells were then incubated at 37 °C in an incubator with humidification containing 5% CO_2. Following incubation, the cells were subjected to 6 different concentrations of AM3, AM4, AM5, AM6, and sorafenib (100, 50, 25, 12.5, 6.25, and 3.125 μM) three times (in triplicate). The plates were incubated under the same conditions for 48 h. MTT dye in phosphate-buffered saline (PBS) was introduced to the wells at a final concentration of 0.5 mg/mL for 4 h. The medium was eliminated, and 200 µL of solubilizing buffer was introduced to each well. The plates were analyzed with a NanoMabna® spectrophotometer at 570 nm.

Statistical analysis

The data were presented as means ± SD and analyzed with GraphPad Prism™ software using one-way analysis of variance (ANOVA) and then Dunnett's post-hoc tests. *P*-values ≤ 0.05 indicate statistical significance.

RESULTS

Chemistry

Ethyl 2-((5-(pyridine-3-yl)-1,3,4-oxadiazol-2-yl)thio)acetate (AM1)

White fluffy powder; yield: 60%; melting point (MP): 65-67 °C; (Rf) = 0.6 (hexane: ethyl acetate: methanol 60%: 30%: 10%); FT-IR (υ, cm^{-1}): 3074 Ar (C–H) str, 2993, 2916 aliph. (CH_2) str, 1735 (C=O) str, 1600 (C=N) str, 1573 Ar (C=C) str, 1195 (C–O) str (Fig. S1); ^{1}H-NMR (400 MHz, DMSO, d_6, δ, ppm): δ 9.14 (s, 1H, Ar-H), 8.80 (d, 1H, Ar-H), 8.34 (d, J = 8.1

Hz, 1H, Ar-H), 7.69-7.57 (m, 1H, Ar-H), 4.32 (s, 2H, –SCH_2–), 4.16 (q, J = 7.1 Hz, 2H, –CH_2–), 1.20 (t, *J* = 7.0 Hz, 3H, –CH_3) (Fig. S2); ^{13}C-NMR (126 MHz, DMSO-d_6, δ, ppm) 167.61, 163.62, 163.43, 152.47, 146.97, 133.94, 124.31, 119.53, 61.59, 33.86, 13.97 (Fig. S3).

2-((5-(pyridin-3-yl)-1,3,4-oxadiazol-2-yl)thio) acetohydrazide (AM2)

White powder; yield: 80%; MP: 171-173 °C; Rf = 0.58 (chloroform: ethylacetate: glacial acetic acid 60%: 30%: 10%); FT-IR (υ cm^{-1}): 3302, 3267 (N–H) str of (NH_2), 3120 (N–H) str of sec. amide, 3043, Ar (C–H) str, 1678 (C=O) str of amide (amide I band), 1539 (C=N) str (Fig. S4); ^{1}H-NMR (500 MHz, DMSO-*d*$_6$, δ, ppm): δ 9.45 (s, 1H, –CONH), 8.80 (d, *J* = 3.2 Hz, 1H, Ar-H), 8.35 (d, *J* = 8.0 Hz, 1H, Ar-H), 7.63 (dd, *J* = 8.0, 4.8 Hz, 1H, Ar-H), 4.49 (broad s, 2H, –NH_2), 4.06 (s, 2H, –SCH_2–) (Fig. S5); ^{13}C-NMR (126 MHz, DMSO-d_6, δ, ppm): 165.50, 164.00, 163.43, 152.54, 147.14, 134.06, 124.37, 119.70, 34.10 (Fig. S6).

(E)-N'-benzylidene-2-((5-(pyridin-3-yl)-1,3,4-oxadiazol-2-yl)thio)acetohydrazide (AM3)

White powder; yield: 90%; MP: 225-22 7°C; Rf = 0.23 (hexane: ethyl acetate: methanol 60%:30%:10%); FT-IR (υ cm^{-1}): 3184 (N–H) str of sec. amide, 3055 Ar (C–H) str, 1670 (C=O) str of amide (amide I band), 1600 (C=N) str (Fig. S7); ^{1}H-NMR (500 MHz, DMSO-*d*$_6$, δ, ppm): 11.83, 11.78 (two s, 1H, H-15 conformers), 8.76 (d, *J* = 3.0 Hz, 1H, H-2), 8.03 (s, 1H, H-17), 7.68 (dd, *J* = 7.3, 2.5 Hz, 2H, H-21 and H-23), 7.59 (m, *J* = 8.0, 4.8 Hz, 1H, H-22), 7.42 (m, *J* = 7.5, 5.3, 2.2 Hz, 3H, H-6, H-20 and H-24), 4.67 (s, 2H, H-13) (Fig. S8). ^{13}C-NMR (126 MHz, DMSO-*d*$_6$, δ, ppm): 167.91, 164.18, 163.90, 163.31, 162.70, 152.39, 147.47, 146.97, 144.17, 133.89, 129.99, 128.74, 126.86, 124.23, 119.60, 34.78 (Fig. S9).

(E)-N'-(4-nitrobenzylidene)-2-((5-(pyridin-3-yl)-1,3,4-oxadiazol-2-yl) thio) acetohydrazide (AM4)

Yellow powder; yield: 95%; MP: 239-241 °C; Rf = 0.30 (hexane: ethyl acetate: methanol 60%:30%:10%); FT-IR (υ cm^{-1}): 3309 (N–H) str of *sec*. amide, 3059 Ar (C–H), 2924, 2835 (C–H) str of aliph. (CH_2), 1686 (C=O) str of amide (amide I band), 1600 (C=N) str, 1543, 1350 (N=O) str (Fig. S10); ^{1}H NMR (500 MHz, DMSO-*d*$_6$, δ, ppm): 12.16, 12.10 (two s, 1H, H-15 conformers), 9.10 (s, 1H, Ar-H), 8.77 (d, *J* = 5.3 Hz, 1H, H-2), 8.38-8.25 (m, 3H, H-6, H20 and H-24), 8.12 (s, 1H, H-17), 7.96 (dd, *J* = 8.6, 6.1 Hz, 2H, H-21 and H-23), 7.59 (dd, *J* = 8.3, 4.9 Hz, 1H, H-1), 4.71 (s, 2H, H-13) (Fig. S11); ^{13}C-NMR (126 MHz, DMSO-*d*$_6$, δ, ppm): 168.37, 164.00, 163.39, 152.41, 147.76, 146.98, 145.01, 141.81, 140.03, 133.90, 128.06, 127.82, 124.22, 123.92, 119.56, 34.62 (Fig. S12).

(E)-N'-(4-chlorobenzylidene)-2-((5-(pyridin-3-yl)-1,3,4-oxadiazol-2-yl) thio)acetohydrazide (AM5)

Off-white powder; yield: 80%; MP: 200-203 °C; Rf = 0.28 (hexane: ethyl acetate: methanol 60%: 30%: 10%); FT-IR (υ cm^{-1}): 3414 (N–H) str of *sec*. amide, 3103 Ar (C–H), 2974 (C–H) str of aliph. (CH_2), 1670 (C=O) str of amide (amide I band), 1608 (C=N) str (Fig. S13); ^{1}H NMR (500 MHz, DMSO-*d*$_6$, δ, ppm): 11.93, 11.88 (two s, 1H, H-15 conformers), 9.10 (s, 1H, H-4), 8.77 (d, *J* = 4.9 Hz, 1H, H-2), 8.31 (d, 1H, H-6), 8.02 (s, 1H, H-17), 7.75–7.67 (m, 2H, H-20 and H-24), 7.60 (m, *J* = 7.4, 4.7 Hz, 1H, H-1), 7.52-7.43 (m, 2H, H-21 and H-23), 4.66 (s, 2H, H-13) (Fig. S14); ^{13}C-NMR (126 MHz, DMSO-*d*$_6$, δ, ppm): 168.53, 164.65, 163.84, 163.33, 152.93, 147.48, 143.36, 134.96, 134.43, 133.22, 129.36, 129.27, 129.03, 124.78, 120.08, 35.29 (Fig. S15).

(E)-N'-(furan-3-ylmethylene)-2-((5-(pyridin-3-yl)-1,3,4-oxadiazol-2-yl)thio)acetohydrazide (AM6)

Light brown powder; yield: 85%; MP: 195-197 °C; RF = 0.27 (hexane: ethyl acetate: methanol 60%: 30%: 10%); FT-IR (υ cm^{-1}): 3178 (N–H) str of sec. amide, 3097 Ar (C–H), 2939, 2816 (C–H) str of ,aliph. (CH_2)1678 (C=O) str of amide (amide I band), 1628 (C=N) str, 1199 (C–O) str (Fig. S16); ^{1}H-NMR (500 MHz, DMSO-*d*$_6$, δ, ppm): 11.67, 11.65 (two s, 1H, H-16 conformers), 9.12 (d, J = 4.8 Hz, 1H, H-4), 8.77 (d, *J* = 2.9 Hz, 1H, H-2), 8.31 (d, *J* = 7.9 Hz, 1H, H-6), 8.12 (S, 1H, H-20), 7.99 (s, 1H, H-18), 7.72 (m, *J* = 6.5 Hz, 1H, H-1), 7.60 (d, *J* = 7.7, 5.8 Hz, 1H, H-22), 6.78 (d, *J* = 1.9 Hz, 1H, H-23), 4.60 (s, 2H, H-13) (Fig. S17); ^{13}C-NMR (126 MHz, DMSO-*d*$_6$, δ, ppm): 167.58, 164.22, 163.30, 152.41, 146.98, 145.27, 144.68, 137.11, 133.92, 124.25, 122.18, 119.59, 107.00, 34.59 (Fig. S18).

Molecular docking study

Sorafenib was used as a reference inhibitor. Sorafenib was docked into the VEGFR-2 for validation, resulting in a root mean square deviation (RMSD) value of 0.208 Å (Fig. 3).

The docking scores (ΔG, kcal/mol) for the compounds evaluated on VEGFR-2 (PDB ID: 4ASD) are presented in Table 1. In the molecular docking study, Fig. 4A-4E illustrates the binding poses of sorafenib and compounds AM3, AM4, AM5, and AM6 to the VEGFR-2.

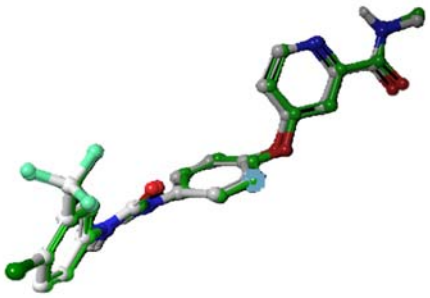

Fig. 3. Sorafenib RMSD

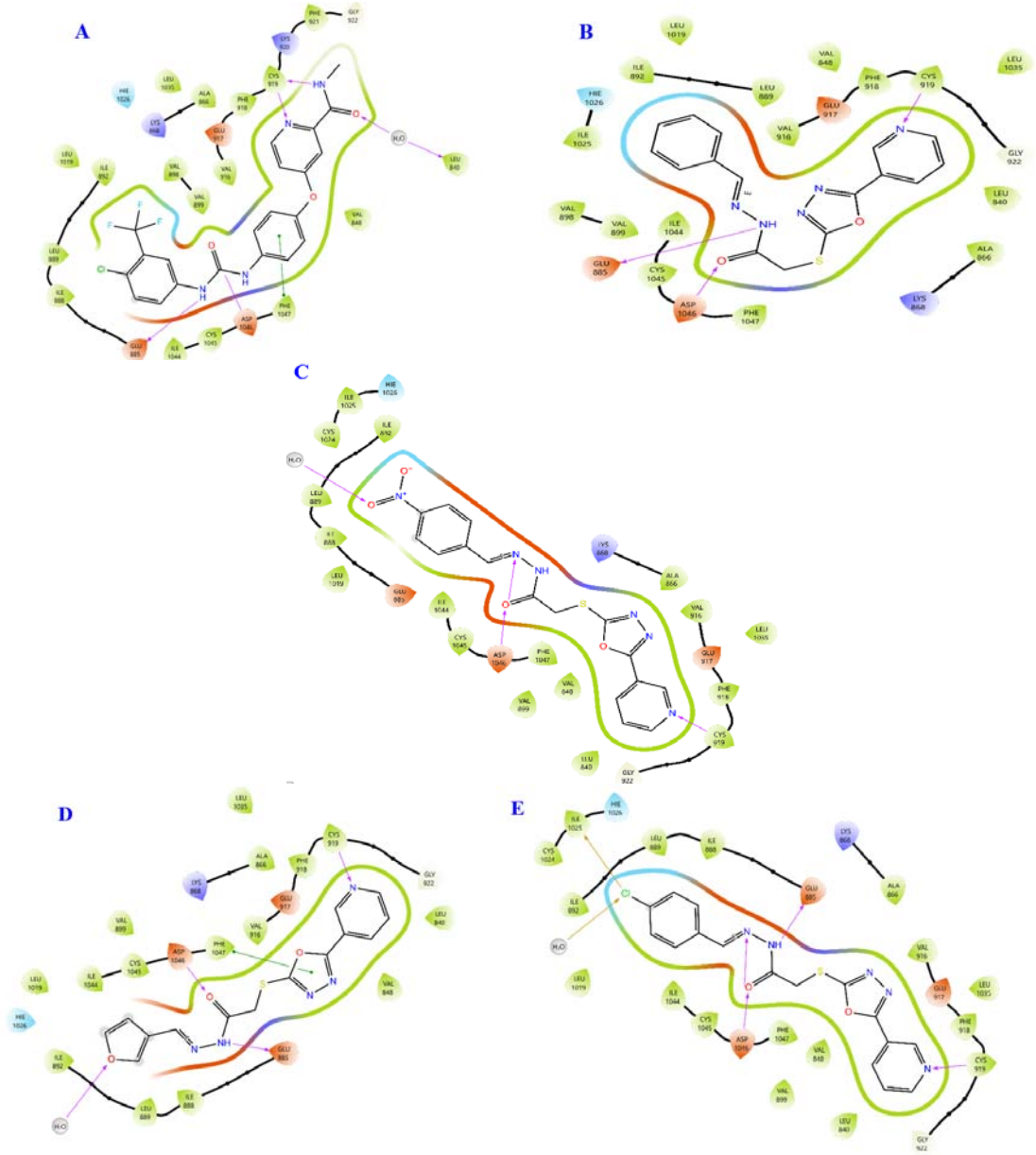

Fig. 4. Docking of the new compounds and the co-crystallized ligand (sorafenib) against the VEGFR-2 binding site (PDB ID: 4ASD). (A) Sorafenib; (B) compound AM3; (C) compound AM4; (D) compound AM5; and (E) compound AM6. VEGFR-2, Vascular endothelial growth factor receptor-2.

Pharmacokinetic properties prediction

Table 2 lists the QikProp predicted characteristics, which offer insights into the ADME characteristics of the final compounds with the reference drug. Molecular weight (MW), octanol/water partition coefficient (QPlogPo/w), prediction of Central Nervous System (CNS) activity, human oral absorption, rule of five, metabolic transformations (#Metab.), hydrogen bond donor (HBD), and hydrogen bond acceptor (HBA) were evaluated.

MD simulation

MD simulations of the compound AM3 in binding with VEGFR2 were conducted for 100 ns using the Desmond tool. The simulation results encompass the RMSD of the complex, the root mean square fluctuation (RMSF) values for both the ligand and the target protein, as well as the protein-ligand interactions observed throughout the simulation period (Fig. 5A-D). In the RMSF analysis of the protein, residues interacting with the ligand are highlighted using green lines. The specific interactions between ligand atoms and protein residues were illustrated in Fig. 6.

MTT in vitro cytotoxicity assay

The newly synthesized compounds (AM3-AM6) were assessed for their *in vitro* cytotoxic effects on HT-29, ACHN, and L929 cell lines. To assess cancer selectivity, the compounds' viabilities in normal cells (L929) were compared with those in cancer cells (HT-29 and ACHN). Table 3 summarizes the obtained IC_{50} values for the cancer cell lines (HT-29 and ACHN) and the selectivity index, which was determined as the ratio of cell viability in normal cells to that in cancer cells. As indicated in Table 3, compound AM4 exhibited the highest cytotoxicity against HT-29 cancer cells, with an IC_{50} value of 38.94 µM, which is the closest to that of the reference drug, sorafenib (IC_{50} = 9.43 µM). Furthermore, Table 3 showed that compounds AM3 and AM4 had the highest selectivity indices against HT-29 and ACHN cells among the compounds.

Table 1. Docking scores (ΔG, kcal/mol) of the tested compounds against the target site (VEGFR-2), PDB ID: 4ASD.

Ligand	Docking score (ΔG, kcal/mol)	Key binding features
AM3	-11.613	H-bond with GLU 885, ASP 1046, and CYS 919
AM6	-11.168	H-bond with GLU 885, ASP 1046, CYS 919 π–π stacking with PHE 1047
AM5	-10.243	H-bond with GLU 885, ASP 1046, and CYS 919; halogen bond with ILE 1025
AM4	-9.525	H-bond with GLU 885, CYS 919
Sorafenib	-11.342	H-bond with GLU 885, ASP 1046, CYS 919, and H_2O; π–π stacking with PHE 1047

Table 2. Predicted pharmacokinetic properties by QikProp for final compounds and sorafenib.

Compound	MW	QPlogpo/w	QPlogBB	Human oral absorption	Rule of five	#Metab	HBD	HBA
AM3	339.37	3.10	-1.01	3	0	4	1	6.5
AM4	384.36	2.25	-2.17	3	0	5	1	7.5
AM5	373.81	3.44	-0.85	3	0	4	1	6.5
AM6	329.33	1.55	-1.35	3	0	5	1	7
Sorafenib	464.83	4.11	-1	1	0	2	3	6

MW, Molecular weight; QPlogPo/w, QikProp-predicted octanol/water partition coefficient; QPlogBB, predicted brain/blood partition coefficient; #Metab, predicted number of likely metabolic reactions; HBA, hydrogen bond acceptor; HBD, hydrogen bond donor.

Table 3. Cytotoxic activity (IC_{50}) and selectivity index of compounds AM3-AM6 against HT-29 and ACHN cancer cells.

Compounds	IC_{50} (μM)		Selectivity index	
	HT-29	ACHN	HT-29	ACHN
AM3	194	443.6	2	2
AM4	38.94	> 1000	2	1.5
AM5	86.54	428.7	2	1.5
AM6	632.4	> 1000	1.5	1
Sorafenib	9.73	15.39	> 3	> 3

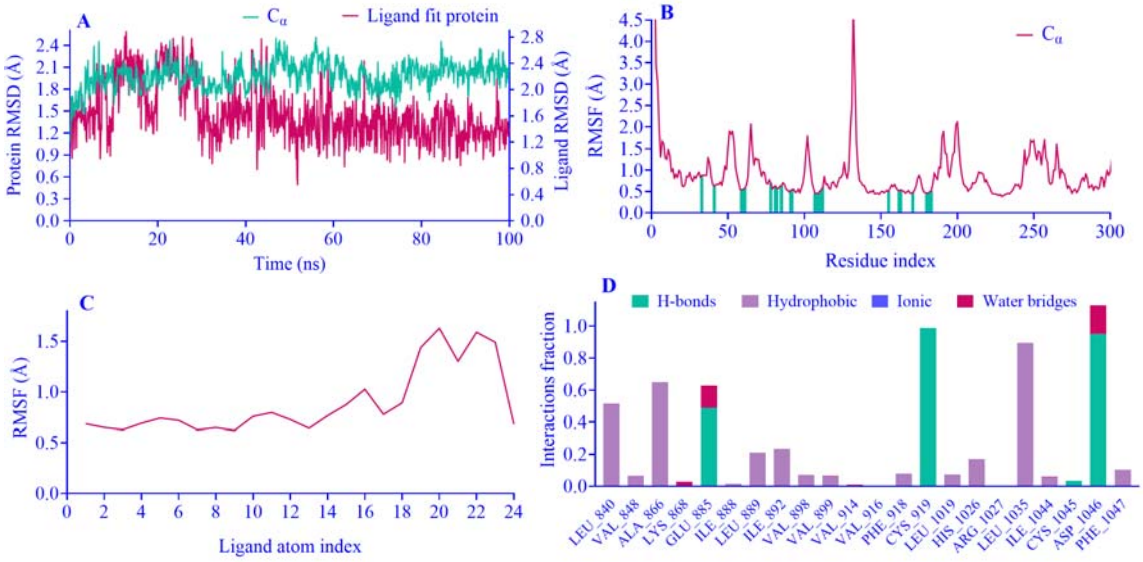

Fig. 5. The molecular dynamics simulation results of AM3 in complex with VEGFR2. (A) Protein ligand RMSD; (B) protein RMSF; (C) ligand RMSF; (D) protein-ligand contacts. VEGFR-2, Vascular endothelial growth factor receptor-2; RMSD, root mean square deviation; RMSF, root mean square fluctuation; Cα, alpha carbon.

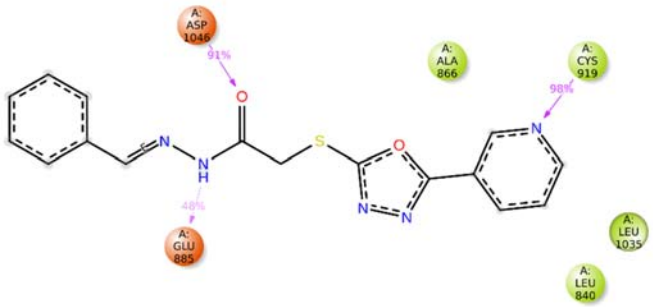

Fig. 6. The specific interactions between ligand atoms and protein residues.

Figure 7A and B illustrate the viability of the compounds against HT-29 (colon cancer) and ACHN (renal cancer) cell lines, respectively, while Fig. 7C presents the results for the normal cell line (L929). Figure 7A shows that most compounds, at most concentrations, significantly reduced the viability of HT-29 cancer cells compared with untreated cells in the control group. Similarly, Fig. 7B shows that compounds have significantly reduced the viability of ACHN cancer cells; notably, all tested concentrations of compound AM4 significantly decreased cell viability. Importantly, Fig. 7C showed that all compounds have maintained the viability of the L929 normal cells at a high percentage.

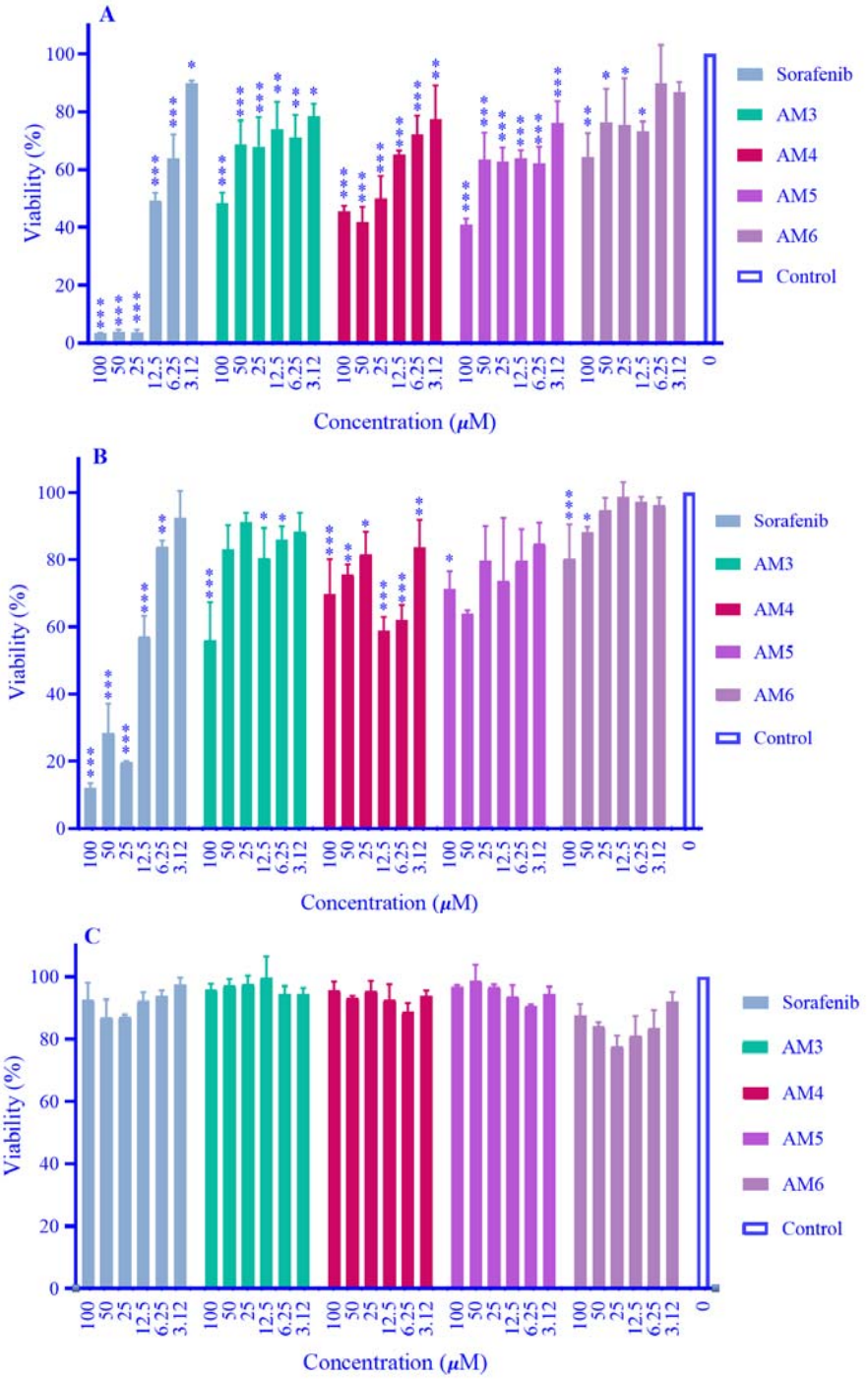

Fig. 7. Viability of compounds on (A) HT-29 colon cancer cells, (B) ACHN renal cancer cells, and (C) L929 normal cells. *$P < 0.05$, **$P < 0.01$, ***$P < 0.01$ indicate significant differences in comparison with the control group.

DISCUSSION

The final compounds showed an excellent affinity for VEGFR-2, as indicated by the docking score values (Table 1). This robust binding is attributed to their interaction with the same key amino acid residues, specifically Glu885 and Asp1046 within the DFG domainand Cys919 in the hinge region, that are essential for the binding mode of the reference compound (sorafenib) (23). This highlights the close alignment between our

compounds and the established inhibitor. Furthermore, a low RMSD value reflects a close alignment between its natural pose and docking pose.

Table 2 presents the expected pharmacokinetic properties of compounds AM3-AM6. The molecular weight range is between 329 and 384 Da, below the 500 Da threshold, favoring oral absorption. The calculated QPlogPo/w values (1.55-3.44) indicate a satisfactory balance between lipophilicity and hydrophilicity, suggesting that the compounds possess sufficient membrane permeability to reach target tissues while maintaining adequate aqueous solubility for systemic circulation, which is critical for *in vivo* efficacy. These values comply with Lipinski's rule, which requires QPlogPo/w < 5. The QPlogBB values (-1.01 to -2.17) indicate limited penetration through the blood-brain barrier, which is a useful property for anticancer drugs not targeting the central nervous system. Regarding metabolic stability, the predicted number of metabolic reactions (#Metab: 4-5) is within the acceptable range for drug-like molecules, indicating that these compounds are unlikely to suffer from rapid first-pass metabolism, thereby supporting reasonable metabolic stability. All compounds demonstrated high calculated oral absorption. All compounds fully comply with Lipinski's rule of five, indicating favourable physicochemical properties for oral bioavailability. Their molecular weights, hydrogen-bond donors and acceptors, and lipophilicity values fall within the acceptable range for drug-like molecules.

MD simulations were conducted to evaluate the stability of the ligand-protein complex and to verify the docking results (Fig. 5). The MD simulation demonstrated the significant stability of the 4ASD-AM3 complex, with the protein C_α RMSD stabilizing between 1.2 and 2.4 Å and the ligand RMSD consistently below 1.5 Å.

The protein RMSF demonstrated significant stability at the binding site, with the interacting residues in the complex exhibiting RMSF values below 2 Å. The low RMSF confirmed that ligand binding effectively rigidified the active site.

The reduced fluctuations observed in compound AM3 contributed to its enhanced stability, allowing it to maintain interactions with VEGFR2 residues for an extended duration, as demonstrated in the protein-ligand contact diagram.

This structural integrity was supported by persistent interactions, notably a frequent water bridge with ASP_1046 (91% occupancy) and a crucial hydrogen bond/ionic interaction with GLU_885.

The findings presented in Figs. 7 and 8 indicate that all newly synthesized compounds exhibited cytotoxicity against two distinct cancer cell lines. Statistical analysis confirmed that all tested concentrations of the oxadiazole derivatives (AM3AM6) induced a significant reduction in cell viability compared to the untreated control, demonstrating a consistent concentration-dependent antiproliferative effect. As shown in Table 3, compound AM4 had the highest cytotoxicity in HT-29 cancer cells, with an IC_{50} value of 38.94 µM. The strong electron-withdrawing effect of the AM4 compound's nitro (NO) moiety (-I effect) primarily accounts for its enhanced potency. The activity profile of the next analogue, AM5, which has a chlorine (Cl) substituent, backs up this conclusion even more. As a halogen, the chlorine group also possesses a significant electron-withdrawing nature, collectively suggesting that the electronic properties of these substituents play a critical role in optimizing the compound's target binding affinity and overall biological efficacy. Crucially, this electronic influence is substantiated by the molecular docking results, which suggest that the nitro group facilitates specific electrostatic or hydrogen-bonding interactions with key active site residues. This specific binding mode helps stabilize the ligand-target complex, offering a structural rationale for the superior potency of AM4 compared to analogues lacking such interacting moieties. It is important to note that due to the limited size of the synthesized series in this preliminary study, these structure-activity observations should be considered preliminary. A larger library of analogs will be required in future stages to establish a robust and definitive SAR profile.

Among the compounds, AM3 and AM4 exhibited the highest selectivity indices against HT-29 and ACHN cells. While these values indicate a moderate selectivity profile compared to the reference drug sorafenib, they identify the current oxadiazole scaffold as a viable starting point for further structural optimization to enhance both potency and the safety margin.

However, *in silico* molecular modelling results only partially correlate with *in vitro* cytotoxicity outcomes, particularly regarding the high binding affinity of AM3 versus the superior cytotoxicity of AM4. This suggests that predicted binding affinities may not fully predict actual cellular responses. This discrepancy could be attributed to factors such as cellular uptake and metabolic stability, which may have favored the bioavailability of AM4, or additional biological mechanisms not captured by the docking and simulation studies. Overall, these findings emphasize the importance of integrating both computational and experimental approaches to obtain a comprehensive understanding of the compounds' anticancer potential and guide future structural optimization efforts.

The synthesis occurred *via* S-alkylation of the thiol group of 5-(pyridin-3-yl)-1,3,4-oxadiazole-2-thiol with ethyl-2-bromoacetate in the presence of triethylamine, yielding compound AM1. AM1 was subsequently treated with hydrazine hydrate, resulting in compound AM2. Compounds (AM3-AM6) were synthesized by refluxing compound (AM2) with different aldehydes to produce imines, which are called Schiff bases (Scheme 1).

The reactions had been monitored using TLC, which ensured that they were completed and the compounds were pure, as the Rf values showed single spots that were positioned differently from the starting materials. The prepared compounds were characterized using FT-IR, ^{1}H-NMR, and ^{13}C-NMR.

The FT-IR spectrum of compound AM1 displayed a stretching vibration at 1735 cm^{-1}, which is characteristic of ester formation (Fig. S1). The characteristic bands of the hydrazide $CONHNH_2$ group were displayed by compound AM2, which was the hydrazinolysis product of compound AM1; these bands include the NH_2 asymmetric stretching vibration at 3302 and 3120 cm^{-1}, the NH amide stretching vibration at 3267 cm^{-1}, the disappearance of the carbonyl group of ester, and the appearance of a strong band at 1678 cm^{-1} indicating hydrazide formation (Fig. S4). The IR analysis of compounds (AM3-AM6) is defined by the absence of hydrazide NH_2 asymmetric stretching and the formation of the (C=N imine) stretching band, which was, in most cases, overlapped with oxadiazole (-C=N-) stretching and is characteristic of compounds (AM3-AM6). Amide (NH) and carbonyl (-C=O) stretching vibrations were observed in their expected regions (Fig. S7, S10, S13, S16).

The ^{1}H-NMR spectrum of compound AM1 shows a singlet at 4.32 ppm corresponding to 2 protons from the –SCH2 group, indicating that it replaced the SH proton as evidence of S-alkylation. The ^{1}H-NMR spectrum of compound AM1 is also characterized by the appearance of protons, which were 2Hs at 4.16 ppm as a quartet and 3Hs at 1.2 ppm as a triplet, which were related to CH_3 and CH_2 groups of $COOCH_2CH_3$, respectively (Fig. S2). The ^{1}H-NMR spectrum of compound AM2 confirmed the replacement of ester protons in compound AM1 (previously seen at 4.16 ppm and 1.2 ppm) with new protons at 9.45 ppm and 4.49 ppm, which correspond to $CONHNH_2$ (Fig. S5). This shows that compound AM1 was successfully hydrazinolyzed. The ^{1}H-NMR spectra of compounds AM3-AM6 exhibited significant structural similarities, particularly in the signals associated with the hydrazide linker (–CONHN–). Due to the restricted rotation around the amide bond, the NH protons appeared as distinct peaks corresponding to *cis* and *trans* conformers. Specifically, these resonances were observed between δ 11.83 and 12.16 ppm for compound AM5 (Fig. S14), and between δ 11.65 and 11.67 ppm for compound AM6 (Fig. S17). A comparable spectral pattern indicating the presence of isomeric mixtures was consistently observed for the remaining analogues (AM3 and AM4), confirming the structural integrity across the entire series. Compounds AM3-AM6 are also characterized by two signals due to syn/anti-syn conformers of imine proton CONHN=C<u>H</u>, at δ 8.21-7.99 ppm. The S-CH_2 group also displayed syn/anti-

syn conformers, resulting in the observation of two distinct signals (Fig. S8, S11, S14, S17) (24).

^{13}C-NMR of compound AM1 is characterized by the appearance of new signals related to (C=O) at 167.61 ppm, to S$\underline{C}$H$_2$ at 33.86 ppm, and to aliphatic CH$_2$ and CH$_3$ of (O$\underline{C}$H$_2\underline{C}$H$_3$) at 61.59 ppm and 13.97 ppm, respectively (Fig. S3). The ^{13}C-NMR spectrum of compound AM2 is characterized by the disappearance of (O$\underline{C}$H$_2\underline{C}$H$_3$) carbons at 61.59 and 13.97 ppm and the shifting of the ($\underline{C}$=O) signal to 165.50 (Fig. S6). The ^{13}C-NMR spectra of the titled compounds (AM3-AM6) also displayed new signals at 143.36-146.97 ppm for the imine moiety ($\underline{C}$H=N) (Fig. S9, S12, S15, S18).

CONCLUSION

In summary, the newly synthesized 5-(pyridine-3-yl)-1,3,4-oxadiazole derivatives have demonstrated remarkable potential as selective VEGFR-2 inhibitors, showing both strong *in silico* binding affinity and promising *in vitro* cytotoxicity against colorectal and renal cancer cell lines. The lead compound, AM3, exhibited exceptional stability within the VEGFR-2 binding site, supported by MD simulations, and the derivatives showed favorable selectivity by sparing normal cell lines.

These findings underscore the considerable promise of this scaffold as a foundation for developing novel anticancer agents. By combining robust computational modelling with thorough biological evaluation, we have identified a compelling new candidate for targeted VEGFR-2 inhibition. The data presented here provide a strong rationale for further preclinical development and optimization, positioning these derivatives as a valuable step toward clinically relevant VEGFR-2-targeted therapies.

Acknowledgments

The authors would like to express their gratitude to the College of Pharmacy, Baghdad University, for providing the necessary laboratory facilities and support to complete this research.

Conflict of interest statement

The authors declared no conflict of interest in this study.

Authors' contributions

M. Oleiwi had the initial concept of the study, designed the research framework, provided scientific supervision, and contributed to manuscript editing and critical revision. A. Abdulhussein performed the literature search, carried out the experimental work and data acquisition, and prepared the first draft of the manuscript. All authors participated in data analysis. All authors have read and approved the finalized article. Each author has fulfilled the authorship criteria and affirmed that this article represents honest and original work.

AI declaration

During the preparation of this work, the authors used Grammarly to improve readability and language. After using this tool, the authors reviewed and edited the content and take full responsibility for its publication.

Supplementary materials

Supplementary materials, including all FT-IR and NMR spectra, are openly available at https://doi.org/10.5281/zenodo.19634497.

REFERENCES

1. Oleiwi MA, Zalzala MH, Khudhair AR, Hadi MK, Abdulazeez ZD. Evaluation of the wound-healing activity and apoptotic induction of new quinazolinone derivatives. Al-Rafidain J Med Sci. 2024;6(2):32-36. DOI: 10.54133/ajms.v6i2.640
2. Siegel RL, Giaquinto AN, Jemal A. Cancer statistics, 2024. CA Cancer J Clin. 2024;74(1):12-49. DOI: 10.3322/caac.21820.
3. Sharma S, Kumar C, Kushwaha H, Jha SK, Chawla S, Sharma A, *et al*. Advancing anticancer drug development: overcoming challenges and exploring new therapeutic strategies. Ayush J Integr Oncol. 2025;2(1):8-27. DOI: 10.4103/ajio.ajio_3_25.
4. Lorenc P, Sikorska A, Molenda S, Guzniczak N, Dams-Kozlowska H, Florczak A. Physiological and tumor-associated angiogenesis: key factors and therapy targeting VEGF/VEGFR pathway. Biomed Pharmacother. 2024;180:117585,1-21. DOI: 10.1016/j.biopha.2024.117585.
5. Lee C, Kim MJ, Kumar A, Lee HW, Yang Y, Kim Y. Vascular endothelial growth factor signaling in health and disease: from molecular mechanisms to

therapeutic perspectives. Signal Transduct Target Ther. 2025;10(1):170,1-40.
DOI: 10.1038/s41392-025-02249-0.
6. Mahaki H, Nobari S, Tanzadehpanah H, Babaeizad A, Kazemzadeh G, Mehrabzadeh M, *et al.* Targeting VEGF signaling for tumor microenvironment remodeling and metastasis inhibition: therapeutic strategies and insights. Biomed Pharmacother. 2025;186:118023,1-16.
DOI: 10.1016/j.biopha.2025.118023.
7. Liu XJ, Zhao HC, Hou SJ, Zhang HJ, Cheng L, Yuan S, *et al*. Recent development of multi-target VEGFR-2 inhibitors for the cancer therapy. Bioorg Chem. 2023;133:106425,1-23.
DOI: 10.1016/j.bioorg.2023.106425.
8. Marques CS, Brandão P, Burke AJ. Targeting vascular endothelial growth factor receptor 2 (VEGFR-2): latest insights on synthetic strategies. Molecules. 2024;29(22):5341,1-49.
DOI: 10.3390/molecules29225341.
9. Khamkar T, Kadam R, Mali SS, Udugade B, Singh S. Recent advances in synthetic approaches for 1, 3, 4-oxadiazole derivatives: a comprehensive review on therapeutic applications. Open Med Chem J. 2025;19(1):e18741045372896,1-16.
DOI: 10.2174/0118741045372896250619051210.
10. Mohamed MFA, Ahmed EA, Alshazly O, Omran OA, Soomro RA, Nafady A. Synthesis, anticancer and anti-inflammatory evaluation of novel quinoxaline-1,3,4-oxadiazole derivatives as EGFR and COX-2 inhibitors. J Mol Struct. 2025;1331:141651,1-12.
DOI: 10.1016/j.molstruc.2025.141651.
11. Tang Z, Hu M, Gan Y, Wen L, Wang Y, Xie Y, *et al*. Design, synthesis, and evaluation of 1, 3, 4-oxadiazole-based EGFR inhibitors. Bioorg Med Chem Lett. 2025;127:130315,1-8.
DOI: 10.1016/j.bmcl.2025.130315.
12. Mishra SS, Samanta A, Paul A, Maji A, Maity TK. Unveiling the anti-cancer potential of oxadiazole derivatives: a comprehensive exploration of structure-activity relationships and chemico-biological insights. Med Chem. 2025;21(6):445-470.
DOI: 10.2174/0115734064329573240823113924.
13. Lata S, Choudhary L, Bharwal A, Pandit A, Abbot V. A comprehensive review: synthesis and pharmacological activities of 1, 3, 4-oxadiazole hybrid scaffolds. Med Chem. 2025;21(10):1051-1071.
DOI: 10.2174/0115734064354700241202174614.
14. Doddagaddavalli MA, Kalalbandi VKA, Seetharamappa J, Joshi SD. New thiophene-1,3,4-oxadiazole-thiazolidine-2,4-dione hybrids: synthesis, MCF-7 inhibition and binding studies. Bioorg Chem. 2024;143:107003. 1-15.
DOI: 10.1016/j.bioorg.2023.107003.
15. Craig RA, De Vicente J, Estrada AA, Feng JA, Lexa KW, Canet MJ, *et al*. Discovery of DNL343: a potent, selective, and brain-penetrant eIF2B activator designed for the treatment of neurodegenerative diseases. J Med Chem. 2024;67(7):5758-5782.
DOI: 10.1021/acs.jmedchem.3c02422.
16. Nath R, Debnath B, Chakraborty A, Khan SA, Maity A, Akhtar MJ. The emerging role of oxadiazole derivatives as VEGFR and EGFR inhibitors in cancer therapy. Bioorg Chem. 2025;166:109140. 1-26.
DOI: 10.1016/j.bioorg.2025.109140.
17. Acar Çevik U, Celik I, Görgülü Ş, Inan Z, Özkay Y, Kaplacıklı Z. New benzimidazole-oxadiazole derivatives as potent VEGFR-2 inhibitors: synthesis, anticancer evaluation, and docking study. Drug Dev Res. 2024;85(4):e22218. 1-10.
DOI: 10.1002/ddr.22218.
18. Osmaniye D, Haji Ali SJ, Korkut Çelikateş B, Ilgın S, Özkay Y, Kaplancıklı ZA. Investigation of anticancer effects of novel piperidine-oxadiazole and piperidine-triazole derivatives as VEGFR inhibitors and evaluation of their molecular docking-dynamic studies. J Mol Struct. 2024;1316:139012. 1-12.
DOI: 10.1016/j.molstruc.2024.139012
19. Hasan Y, Al-hamashi A. Identification of selisistat derivatives as SIRT1-3 inhibitors by in silico virtual screening. Turk Comput Theor Chem. 2023;8(2):1-11.
DOI: 10.33435/tcandtc.1224592
20. Ali R, Al-Hamashi A. Molecular docking, ADMET, molecular dynamic simulation, synthesis, and preliminary antiproliferative study of 1, 2, 4-thiadiazole derivatives as possible histone deacetylase inhibitors. Trop J Pharm Res. 2024;23(7):1069-1076.
DOI: 10.4314/tjpr.v23i7.4.
21. Hadi MK, Abdulkadir MQ, Oleiwi MA, Ahmed S, Kamms ZD. Synthesis, characterization and preliminary antimicrobial study of some new ether and thioether derivatives of sulfadiazine. Iraqi J Pharm Sci. 2025;34(1):176-184.
DOI: 10.31351/vol34iss1pp176-184.
22. Tawfeeq MF, Qassir AJ. Synthesis, characterization, and antibacterial evaluation of new vanillic acid derivatives. Iraqi J Pharm Sci. 2020;29(2):129-138.
DOI: 10.31351/vol29iss2pp129-138.
23. Chaudhari PJ, Nemade AR, Shirkhedkar AA. Recent updates on potential of VEGFR-2 small-molecule inhibitors as anticancer agents. RSC Adv. 2024;14(45):33384-33417.
DOI: 10.1039/d4ra05244g.
24. Fernández-Palacios S, Matamoros E, Morato Rojas I, López Navarrete JT, Ruiz Delgado MC, Vida Y, *et al*. New insights into acylhydrazones e/z isomerization: an experimental and theoretical approach. Int J Mol Sci. 2023;24(19):14739,1-17.
DOI: 10.3390/ijms241914739.